CHINESE OPTICS LETTERS

Vol. 21, No. 2 | February 2023

Hundred-watt level high-order mode all-fiberized random distributed feedback Raman fiber laser with high mode purity

Yang Li (李 阳)[1], Xiulu Hao (郝修路)[1], Yi An (安 毅)[1], Yi Zhu (朱 毅)[2], Tianfu Yao (姚天甫)[1*], Xianglong Zeng (曾祥龙)[2**], and Pu Zhou (周 朴)[1]

[1] College of Advanced Interdisciplinary Studies, National University of Defense Technology, Changsha 410073, China

[2] Key Laboratory of Specialty Fiber Optics and Optical Access Networks, Joint International Research Laboratory of Specialty Fiber Optics and Advanced Communication, Shanghai Institute for Advanced Communication and Data Science, Shanghai University, Shanghai 200444, China

*Corresponding author: yantianfumary@163.com

**Corresponding author: zenglong@shu.edu.cn

Received July 24, 2022 | Accepted August 30, 2022 | Posted Online October 12, 2022

An all-fiberized random distributed feedback Raman fiber laser (RRFL) with LP_{11} mode output at 1134 nm has been demonstrated experimentally, where an intracavity acoustically induced fiber grating is employed for modal switching. The maximum output power of LP_{11} mode is 93.8 W with the modal purity of 82%, calculated by numerical mode decomposition technology based on stochastic parallel-gradient descent algorithm. To our best knowledge, this is the highest output power with high purity of LP_{11} mode generated from the RRFL. This work may pave a path towards advanced fiber lasers with special temporal and spatial characteristics for applications.

Keywords: acoustically induced fiber grating; LP_{11} mode; mode decomposition; random distributed feedback Raman fiber laser.

DOI: 10.3788/COL202321.021406

1. Introduction

Fiber lasers with effective modal control to achieve specific high-order modes (HOMs) output have attracted much attention in the past few decades, thanks to their unique polarization, amplitude, and phase characteristics, which have been applied to mode division multiplexing[1], industrial processing[2], and so on. Moreover, further generation of cylindrical vector beams and vortex beams based on HOMs has also been verified[3–9], which finds a tremendous range of applications, including plasmon excitation[10], optical tweezers[11], and electron acceleration[12]. So far, several routines to achieve HOMs have been confirmed, such as specially designed fibers[13,14], lateral offset splicing[15], long-period fiber gratings (LPFGs)[16–18], few-mode fiber Bragg gratings (FMFBGs)[19–22], mode-selective couplers (MSCs)[4,23–27], spatial light modulators[28–32], active polarization control[33,34], and acoustically induced fiber gratings (AIFGs)[35–38].

Among those techniques above, fiber-based methods have shown great potential for power scaling of HOMs generation in all-fiberized systems, which are in demand in most practical applications. For example, Abedin *et al.* realized 100 W output of $LP_{0,10}$ mode based on specially designed Yb:HOM fiber[14]. Furthermore, Su *et al.* demonstrated a mode-switchable high-power all-fiber master oscillation power amplification (MOPA) system with the LP_{11} output power at the 500 W level by regulating the input polarization state of the seed laser at 1060 nm[33]. Later in 2019, You *et al.* used similar methods and achieved ~1.4 kW output at 1060 nm with LP_{11} modal purity of 78%, which is the highest power of LP_{11} mode in continuous-wave fiber lasers[34]. Recently, Wu *et al.* utilized the AIFG to accomplish a hundred-watt mode switchable laser based on the Yb-doped MOPA scheme.

Nevertheless, one could find that most of the demonstrations above are based on rare-earth-doped fiber lasers, whose emission bands are highly restricted. In recent years, new applications have been continuously derived from lasers of HOMs, making precise wavelength manipulation of greater significance. For example, the combination of wavelength division multiplexing and mode division multiplexing can increase the transmission capacity of the communication system exponentially[39]. To broaden the spectral window, the laser gain mechanism based on the stimulated Raman scattering (SRS) effect in purely passive fiber is expected to be a good solution, including Raman fiber

laser (RFL)[40] and random distributed feedback Raman fiber laser (RRFL)[41]. In 2013, Jocher *et al.* demonstrated an RFL at 1115 nm, achieving azimuthally and radially polarized beams by controlling the polarization of a Gaussian pump beam[42]. Compared with RFL, the RRFL has the advanced features of low coherence and simple structure, thanks to the random distributed feedback scheme provided by Rayleigh scattering. So far, RRFLs reported have predominantly utilized single-mode fibers (SMFs) with core pumping configuration, thus realizing single-transverse-mode output. Notwithstanding, RRFLs with different spatial modes have outstanding advantages in many practical applications, such as reducing laser speckle[43], lowering turbulence-induced scintillation in free-space optical communication[44], and a ghost-imaging technique that is not affected by meteorological conditions[45]. The first exploration was reported by Du *et al.* in 2015[15], realizing switchable output between the LP_{01} and LP_{11} modes in RRFL at 1070 nm by employing an offset splicing spot and two polarization controllers, while the power of LP_{11} mode was only 10 mW with a slope efficiency less than 1% due to the high loss introduced by the splicing spot. In order to improve efficiency, Lv *et al.* utilized a piece of annular doping Yb-doped fiber together with passive fiber to enhance the gain of LP_{11} mode in RRFL[46]. The slope efficiency increased to 7.2% with a maximum output of 17 mW at 1055 nm, and the power level is still far from the practical requirement.

In this paper, we experimentally demonstrated a high-power all-fiberized RRFL with high-purity LP_{11} mode at 1134 nm. The mode conversion was achieved by employing an intracavity AIFG due to its wavelength tunability and fast conversion speed. The maximum signal light output power of the LP_{01} mode and LP_{11} mode is 96.6 W and 93.8 W, respectively. It is noticeable that the average purity of LP_{11} mode is as high as 82%, which is decomposed based on the stochastic parallel gradient descent (SPGD) algorithm. To the best of our knowledge, it is the highest power of high purity of LP_{11} mode generated from RRFL. For potential industry applications, the stability of the system was also verified with good results in 20 min.

2. Experimental Setup

2.1. Characteristics of AIFG

The AIFG is the key component to generate LP_{11} mode in RRFL. As shown in Fig. 1(a), the basic structure of AIFG consists of a piezoceramic transducer (PZT) with a quartz horn and a piece of few-mode fiber (FMF) attached. The PZT is driven by a periodic electrical signal with high amplitude generated from the radio-frequency (RF) source, including an electrical signal generator and a voltage amplifier inside. When the periodic electrical signal loads, the PZT starts to vibrate, and the vibration is transmitted to FMF by the quartz horn. Then the acoustic wave caused by vibration further modulates the refractive index of FMF periodically, similar to the LPFG structure, whose grating period can be calculated by the following formula[35,47]:

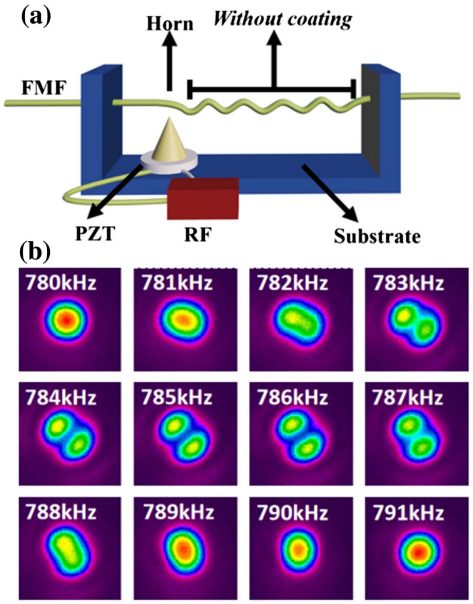

Fig. 1. (a) Constructions of AIFG. FMF, few-mode fiber; PZT, piezoceramic transducer; RF, radio-frequency source. (b) Output beam profiles of 1130 nm laser at different frequencies.

$$\Lambda = \sqrt{\pi R C_{\text{ext}}/f}, \tag{1}$$

where R is the cladding radius of the FMF, $C_{\text{ext}} = 5760$ m/s is the propagation velocity of acoustic wave in the quartz fiber, and f is the frequency of the loading signal and the acoustic wave.

According to the mode-coupling theory, the modes can be coupled when the following phase-matching condition is matched[48]:

$$\Lambda = L_B = \lambda/(n_{01} - n_{11}), \tag{2}$$

where λ is the wavelength of transmitted laser, and n_{01} and n_{11} represent the effective refractive indices of LP_{01} and LP_{11} mode propagating along the fiber, respectively. Hence, the input guided fundamental mode LP_{01} in FMF would be converted to higher-order mode LP_{11} at output.

Based on the principle of AIFG, in order to achieve efficient mode conversion, the loaded signal frequency of AIFG needs to be adjusted to satisfy mode-coupling conditions. To test the correspondence between the loaded signal frequency and the generated beam profile, the output beam profiles directly after the AIFG are measured first by injecting a laser signal at 1130 nm, as shown in Fig. 1(b). When the frequency increases from 780 kHz, the output beam profile gradually evolves from LP_{01} mode to LP_{11} mode until the appearance of the most obvious LP_{11} mode spot, corresponding to the eigenfrequency of 785 kHz. Then the frequency increases further, and the spot returns to LP_{01} mode. This means that the AIFG could not only switch the two modes, but also change their ratio by varying the frequency.

Furthermore, the LP_{01}-mode transmission spectra of the AIFG are tested by a broadband light source, and some results are shown in Fig. 2(a). These discrete peaks do not imply that

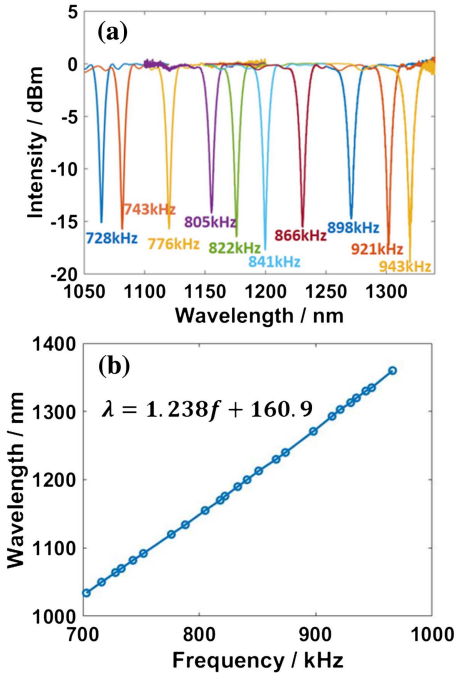

Fig. 2. (a) Transmission spectrum of LP_{01} mode at different loaded frequencies; (b) fitted curve between eigenfrequency and wavelength.

efficient mode conversion only occurred at these wavelengths. In fact, at any wavelength from 1050 to 1300 nm, we can always obtain an optimum frequency that makes the transmission curve of LP_{01} mode reach more than 15 dB, indicating a high mode conversion efficiency from LP_{01} mode to LP_{11} mode. As shown in Fig. 2(a), the modal conversion shifts to longer wavelengths when frequency increases, and their relationship is shown in Fig. 2(b). The fit curve satisfies the following linear expression:

$$\lambda = 1.238f + 160.9, \tag{3}$$

where λ is the wavelength (in nanometers) and f is the loaded frequency (in kilohertz).

2.2. Setup of RRFL with controllable mode

In order to generate controllable output beam profiles, the experimental setup of the RRFL is designed as shown in Fig. 3(a). An ytterbium-doped fiber laser (YDFL) operating at 1080 nm with a maximum output power of 120 W is utilized as the pump source. The half-open cavity of RRFL is formed by a high-reflection (HR) fiber Bragg grating (FBG), a piece of FMF, and a fiber end cap. The HR FBG is written in the FMF with a reflectance of more than 99.5% at 1134 nm. The end cap is antireflection-coated to evade unwanted end feedback. As shown in Fig. 3(b), the FMF is commercial graded-index (GRIN) fiber with a parabolic profile of the refractive index, providing both Raman gain and distributed feedback. The core diameter and numerical aperture (NA) of the FMF are 20 μm and 0.14 separately, with a length of 400 m that has been optimized thoroughly to achieve high efficiency. The HR FBG is

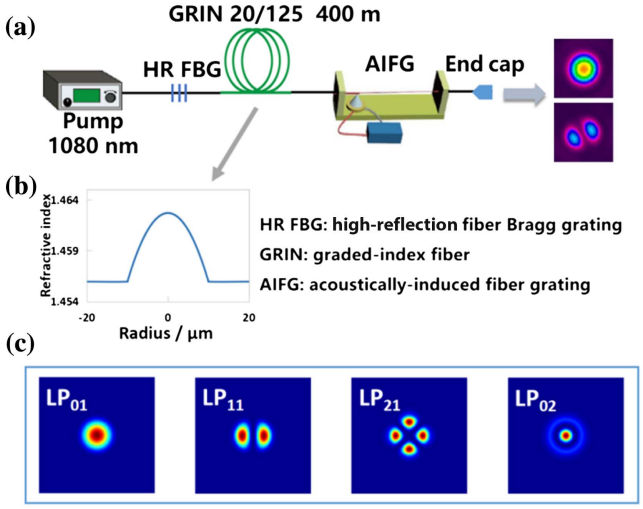

Fig. 3. (a) Experimental setup of mode controllable RRFL; (b) refractive index of GRIN FMF; (c) four LP modes supported at both 1080 and 1134 nm.

written in the same GRIN FMF, which guarantees the mode field matching at the fusion splices in the laser. The AIFG described in the last section is located between the FMF and the fiber end cap to modify the generated mode. The fiber used in AIFG is step-index FMF with a core diameter and an NA of 16 μm and 0.11 separately, indicating four LP modes supported in the core at both 1080 and 1134 nm, as shown in Fig. 3(c).

3. Results and Discussion

3.1. Laser output power and spectrum

Figure 4(a) exhibits the output signal power as a function of the pump power with the corresponding output beam spot inserted. By switching on/off the RF source operating at 787 kHz, which was precisely the eigenfrequency of 1134 nm, the mode conversion can be achieved. The red and the black lines refer to the LP_{01} mode and LP_{11} mode signal light being output individually. It can be observed that the output power of LP_{11} mode is always slightly lower than that of LP_{01} mode at the same pump power as a result of the loss in the mode conversion process. It is worth noting that the growth curve of output signal power is not straight. When the pump power exceeds the threshold of around 42 W, but is below 60 W, the signal power grows rapidly and the light-to-light conversion efficiency even exceeds 100%. This phenomenon has been explained by numerical calculation in detail in Ref. [41]. Indeed, in the RRFL with forward-pumped configuration, the highest power and efficiency are reached in a short fiber, despite the generation threshold being relatively high. Then, when the pump power exceeds 60 W, the power evolution curves of the LP_{01} and LP_{11} modes are approximately linear, with the slope efficiency of 93.8% and 90.3%. The maximum output power of LP_{01} mode and LP_{11} mode is 96.6 W and 93.8 W independently. Figure 4(b) illustrates the spectra at different output power levels for LP_{01} and LP_{11} modes. The central

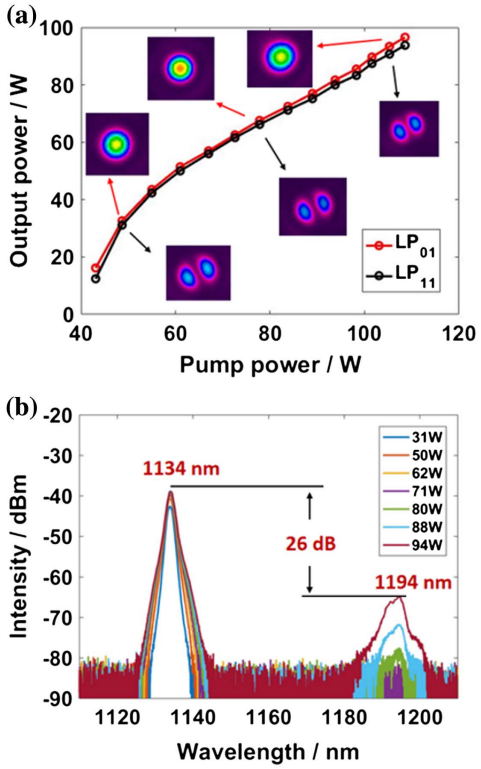

Fig. 4. (a) Output signal power as a function of pump power and beam spots; (b) spectrum at different output power levels for LP_{01} and LP_{11} modes.

wavelength of the signal is 1134 nm, while the second-order Raman–Stokes wavelength is 1194 nm. At the maximum output power, the intensity of the second-order Stokes is 26 dB lower than that of the signal light, limiting further power scaling. Since the mode conversion is executed near the output end, there were not many differences in spectra in both working states.

3.2. Modal decomposition on modal content

The output modal content can be decomposed numerically by the method of MD based on the SPGD algorithm[49,50]. The output beam profiles of the Raman laser at 1134 nm are captured at the focal plane by a CCD camera. Figure 5(a) shows the measured and reconstructed beam profiles at different power levels, respectively. The correlation coefficient J, defined as the similarity between actual and reconstructed beam profiles, remains above 0.99 in all results, indicating the high accuracy of MD. In addition, the purity of the LP_{11} remains around 80%, which means that the AIFG could achieve mode conversion effectively. Figure 5(b) shows the content of the LP_{01}, LP_{11} modes and the other modes (LP_{21} and LP_{02}) at the highest power, from which we can see that in addition to the first two orders, the content of other modes is extremely low. For potential practical applications, the stability of output LP_{11} mode is also tested. Figure 5(c) exhibits the MD results, which are recorded every 2 min. The content of the LP_{01} mode and the LP_{11} mode remained comparatively stable within 20 min, with an average purity of LP_{11} mode of 82%. Furthermore, the system was stable with good

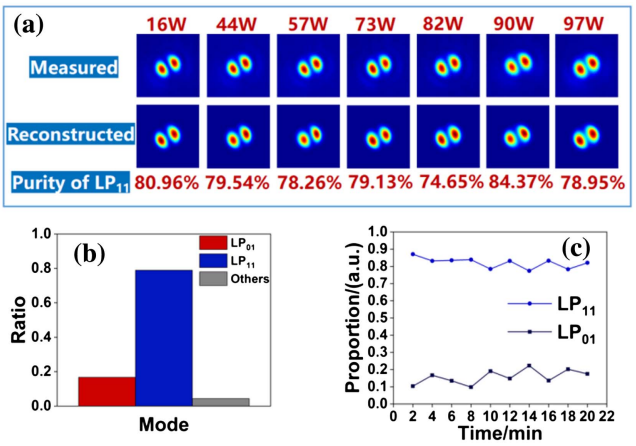

Fig. 5. (a) Measured and reconstructed beam profiles as well as calculated mode purity at different power levels; (b) content of the LP_{01}, LP_{11} modes and the other modes at the highest power; (c) MD results of RRFL recorded every 2 min in 20 min.

repeatability, and none of the degradation of beam spots, spectrum, and power fluctuation was observed, even after the test time.

Thanks to the flexible mode control property of AIFG, the laser also possesses agile mode-switching capability. The switching time has been intensively studied. By placing a pinhole attached to a photon detector (PD), the detected intensity got changed once the spots changed, which means mode switching. The position of the pinhole should be adjusted carefully to make it close to the center of the beam profile, so that intensity changes can be detected when the mode changed. By capturing the rising edge of the temporal trace, the switching time from LP_{01} to LP_{11} mode is about 0.8 ms, as shown in Fig. 6(a). Likewise, the switching time from LP_{11} to LP_{01} mode can be obtained by capturing the falling edge of the temporal trace, which is still about 0.8 ms, as shown in Fig. 6(b). The switching time is mainly determined by the transit time of the acoustic flexural wave propagating through the acousto-optic coupling region of the AIFG, which could be further reduced if the acousto-optic coupling length was reduced.

In Table 1, a performance comparison of RRFLs aimed at generating HOMs is presented. In this table, we mainly take into account the method of achieving HOMs, maximum output power, and the slope efficiency in the references used in this

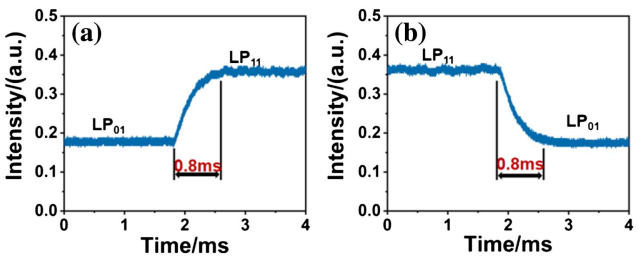

Fig. 6. (a) Rising and (b) falling edge of the temporal trace.

Table 1. Performance Comparison of RRFLs Generating HOMs.

Method	Maximum Power	Slope Efficiency	Reference
Lateral offset splicing	10 mW	< 1%	[15]
LPFG	77.9 μW	0.0037%	[16]
FM-FBG	17.17 mW	7.2%	[46]
MSC	< 10 mW	3.3%	[51]
AIFG	93.8 W	> 90%	This paper

paper. The comparison shows that the proposed RRFL in this paper has a relatively high slope efficiency and more than 2 orders of magnitude improvement in power level. The mode purity and switching time are not listed in Table 1, as most of other studies did not give the results.

4. Conclusion

In conclusion, we presented the experimental demonstration of swift and adaptive mode conversion between LP_{01} and LP_{11} modes in RRFL by applying an AIFG in the half-open cavity. The AIFG is a fast mode converter, and the switching time is as short as 0.8 ms. The maximum output power of the LP_{01} and LP_{11} modes is 96.6 and 93.8 W, respectively, with a high efficiency of over 90%. The MD technique based on SPGD algorithm is applied to calculate the mode purity, which is up to 82% for the LP_{11} mode. To our best knowledge, it is the first time that mode switching in RRFL using MD has been analyzed, and it is also the highest power of LP_{11} mode generated from RRFL. This experiment breaks through the power level that the AIFG can withstand directly rather than through the MOPA structure and also proves its superior performance at the hundred-watt level. The system has the advantages of small insertion loss, fast conversion speed, and good robustness, which gives it good potential in application. To achieve higher-order mode control and higher output power, further optimization of the laser system will be demonstrated. This work may lay a foundation for fiber lasers with special temporal and spatial characteristics for applications in the fields of mode division multiplexing, imaging, and laser material processing.

Acknowledgement

This work was supported by the National Natural Science Foundation of China (Nos. 11704409, 62061136013, and 12174445), the Open Research Fund of State Key Laboratory of Pulsed Power Laser Technology (No. SKL2020KF03), and the Special Fund for Hunan Provincial Innovative Province Building (No. 2019RS3017).

References

1. P. Lu, M. Shipton, A. Wang, S. Soker, and Y. Xu, "Adaptive control of waveguide modes in a two-mode-fiber," Opt. Express **22**, 2955 (2014).
2. R. Weber, A. Michalowski, M. Abdou-Ahmed, V. Onuseit, V. Rominger, M. Kraus, and T. Graf, "Effects of radial and tangential polarization in laser material processing," Phys. Procedia **12**, 21 (2011).
3. W. Fang, R. Tao, Y. Zhang, H. Li, P. Jun, and L. Xu, "Adaptive modal gain controlling for a high-efficiency cylindrical vector beam fiber laser," Opt. Express **27**, 32649 (2019).
4. M. Huang, J. Wu, J. Hong, H. Lei, C. Zhao, Y. Chen, and D. Fan, "High energy switchable pulsed high-order mode beams in a mode-locking Raman all-fiber laser with high efficiency," Opt. Express **29**, 40538 (2021).
5. H. Li, K. Yan, Y. Zhang, C. Gu, P. Yao, L. Xu, R. Zhang, J. Su, W. Chen, and Y. Zhu, "Low-threshold high-efficiency all-fiber laser generating cylindrical vector beams operated in LP11 mode throughout the entire cavity," Appl. Phys. Express **11**, 122502 (2018).
6. D. Mao, Y. Zheng, C. Zeng, H. Lu, C. Wang, H. Zhang, W. Zhang, T. Mei, and J. Zhao, "Generation of polarization and phase singular beams in fibers and fiber lasers," Adv. Photonics **3**, 014002 (2021).
7. W. Jian, C. S. Chen, and L. Jun, "Orbital angular momentum communications based on standard multi-mode fiber," APL Photonics **6**, 060804 (2021).
8. H. Tong, G. Xie, Z. Qiao, Z. Qin, P. Yuan, J. Ma, and L. Qian, "Generation of a mid-infrared femtosecond vortex beam from an optical parametric oscillator," Opt. Lett. **45**, 989 (2020).
9. Z. Qiao, Z. Wan, G. Xie, J. Wang, L. Qian, and D. Fan, "Multi-vortex laser enabling spatial and temporal encoding," Photoni X **1**, 13 (2020).
10. A. Bouhelier, F. Ignatovich, A. Bruyant, C. Huang, G. Colas des Francs, J.-C. Weeber, A. Dereux, G. P. Wiederrecht, and L. Novotny, "Surface plasmon interference excited by tightly focused laser beams," Opt. Lett. **32**, 2535 (2007).
11. G. Volpe, G. P. Singh, and D. Petrov, "Optical tweezers with cylindrical vector beams produced by optical fibers," Proc. SPIE **5514**, 283 (2004).
12. D. N. Gupta, N. Kant, D. E. Kim, and H. Suk, "Electron acceleration to GeV energy by a radially polarized laser," Phys. Lett. A **368**, 402 (2007).
13. H. Li, Y. Zhang, Z. Dong, J. Lv, C. Gu, P. Yao, L. Xu, R. Zhang, J. Su, W. Chen, Y. Zhu, and Q. Zhan, "A high-efficiency all-fiber laser operated in high-order mode using ring-core Yb-doped fiber," Ann. Phys. **531**, 1900079 (2019).
14. K. S. Abedin, R. Ahmad, A. M. Desantolo, and D. J. Digiovanni, "Reconversion of higher-order-mode (HOM) output from cladding-pumped hybrid Yb:HOM fiber amplifier," Opt. Express **27**, 8585 (2019).
15. X. Du, H. Zhang, P. Ma, X. Wang, P. Zhou, and Z. Liu, "Spatial mode switchable fiber laser based on FM-FBG and random distributed feedback," Laser Phys. **25**, 095102 (2015).
16. M. Zulkifli, K. Lau, F. Muhammad, and M. Yasin, "Dual-mode output in half open cavity random fibre laser," Opt. Commun. **430**, 273 (2019).
17. J. Tao, L. Wang, L. Zhang, L. Teng, Z. Zhang, R. Berko, L. Zhang, F. Pang, and X. Zeng, "Dynamic mode-switchable and wavelength-tunable Brillouin random fiber laser by a high-order mode pump," Opt. Express **29**, 34109 (2021).
18. P. Steinvurzel, K. Tantiwanichapan, M. Goto, and S. Ramachandran, "Fiber-based Bessel beams with controllable diffraction-resistant distance," Opt. Lett. **36**, 4671 (2011).
19. J. Song, H. Xu, H. Wu, L. Huang, J. Xu, H. Zhang, and P. Zhou, "High power narrow linewidth LP_{11} mode fiber laser using mode-selective FBGs," Laser Phys. Lett. **15**, 115101 (2019).
20. B. Sun, A. Wang, L. Xu, C. Gu, Z. Lin, H. Ming, and Q. Zhan, "Low-threshold single-wavelength all-fiber laser generating cylindrical vector beams using a few-mode fiber Bragg grating," Opt. Lett. **37**, 464 (2012).
21. L. Li, M. Wang, T. Liu, J. Leng, P. Zhou, and J. Chen, "High power, cladding-pumped all-fiber laser with selective transverse mode generation property," Appl. Opt. **56**, 4967 (2017).
22. T. Liu, S. Chen, and J. Hou, "Selective transverse mode operation of an all-fiber laser with a mode-selective fiber Bragg grating pair," Opt. Lett. **41**, 5692 (2016).
23. T. Wang, F. Shi, Y. Huang, J. Wen, Z. Luo, F. Pang, T. Wang, and X. Zeng, "High-order mode direct oscillation of few-mode fiber laser for high-quality cylindrical vector beams," Opt. Express **26**, 11850 (2018).
24. F. Wang, F. Shi, T. Wang, F. Pang, T. Wang, and X. Zeng, "Method of generating femtosecond cylindrical vector beams using broadband mode converter," IEEE Photonics Technol. Lett. **29**, 747 (2017).

25. J. Wang, H. Wan, H. Cao, Y. Cai, B. Sun, Z. Zhang, and L. Zhang, "A 1-μm cylindrical vector beam fiber ring laser based on a mode selective coupler," IEEE Photonics Technol. Lett. **30**, 765 (2018).
26. S. Chen, W. Hu, Y. Xu, Y. Cai, Z. Wang, and Z. Zhang, "Mode-locked pulse generation from an all-FMF ring laser cavity," Chin. Opt. Lett. **17**, 121405 (2019).
27. C. Dong, J. Zou, H. Wang, H. Yao, X. Zeng, Y. Bu, and Z. Luo, "Visible-light all-fiber vortex lasers based on mode selective couplers," Chin. Phys. B **29**, 161 (2020).
28. Y. Jung, Z. Li, N. Wong, J. Daniel, J. Sahu, S. Alam, and D. Richardson, "Spatial mode switchable, wavelength tunable erbium doped fiber laser incorporating a spatial light modulator," in *Optical Fiber Communications Conference* (2014), p. 1.
29. A. Forbes, A. Dudley, and M. McLaren, "Creation and detection of optical modes with spatial light modulators," Adv. Opt. Photonics **8**, 200 (2016).
30. C. Tian, S. Yu, S. Cai, M. Lan, and W. Gu, "Fiber laser for on-demand mode generation in 1550 nm band," Photonics Res. **5**, 256 (2017).
31. D. Lin, J. Carpenter, Y. Feng, S. Jain, Y. Jung, Y. Feng, M. N. Zervas, and D. J. Richardson, "Reconfigurable structured light generation in a multicore fibre amplifier," Nat. Commun. **11**, 3986 (2020).
32. X. Ma, J. Ye, Y. Zhang, J. Xu, J. Wu, T. Yao, J. Leng, and P. Zhou, "Vortex random fiber laser with controllable orbital angular momentum mode," Photonics Res. **9**, 266 (2021).
33. R. Su, B. Yang, X. Xi, P. Zhou, X. Wang, Y. Ma, X. Xu, and J. Chen, "500 W level MOPA laser with switchable output modes based on active control," Opt. Express **25**, 23275 (2017).
34. Y. You, G. Bai, X. Zou, X. Li, M. Su, H. Wang, Z. Quan, M. Liu, J. Zhang, Q. Li, H. Shen, Y. Qi, B. He, and J. Zhou, "A 1.4-kW mode-controllable fiber laser system," J. Light. Technol. **39**, 2536 (2021).
35. J. Xu, L. Zhang, X. Liu, L. Zhang, J. Lu, L. Wang, and X. Zeng, "Dynamic vortex mode-switchable erbium-doped Brillouin laser pumped by high-order mode," Opt. Lett. **46**, 468 (2021).
36. W. Zhang, L. Huang, K. Wei, P. Li, B. Jiang, D. Mao, F. Gao, T. Mei, G. Zhang, and J. Zhao, "High-order optical vortex generation in a few-mode fiber via cascaded acoustically driven vector mode conversion," Opt. Lett. **41**, 5082 (2016).
37. X. Zhang, W. Zhang, C. Li, D. Mao, F. Gao, L. Huang, D. Yang, T. Mei, and J. Zhao, "All-fiber cylindrical vector beams laser based on an acoustically-induced fiber grating," J. Opt. **20**, 075608 (2018).
38. H. Wu, J. Xu, L. Huang, X. Zeng, and P. Zhou, "High-power fiber laser with real-time mode switchability," Chin. Opt. Lett. **20**, 021402 (2022).
39. Y. Yang, Y. Li, Y. Huang, and A. W. Poon, "Silicon nitride three-mode division multiplexing and wavelength-division multiplexing using asymmetrical directional couplers and microring resonators," Opt. Express **22**, 22172 (2014).
40. V. R. Supradeepa, Y. Feng, and J. W. Nicholson, "Raman fiber lasers," J. Opt. **19**, 023001 (2017).
41. S. K. Turitsyn, S. A. Babin, A. E. El-Taher, P. Haraper, D. V. Churkin, S. I. Kablukov, J. D. Ania-Castanon, V. Karalekas, and E. V. Podivilov, "Random distributed feedback fibre laser," Nat. Photonics **4**, 231 (2010).
42. C. Jocher, C. Jauregui, M. Becker, M. Rothhardt, J. Limpert, and A. Tünnermann, "An all-fiber Raman laser for cylindrical vector beam generation," Laser Phys. Lett. **10**, 125108 (2013).
43. R. Ma, J. Li, J. Guo, H. Wu, H. Zhang, B. Hu, Y. Rao, and W. Zhang, "High-power low spatial coherence random fiber laser," Opt. Express **27**, 8738 (2019).
44. W. Cheng, J. Haus, and Q. Zhan, "Propagation of vector vortex beams through a turbulent atmosphere," Opt. Express **17**, 17829 (2009).
45. H. Wu, B. Han, Z. Wang, G. Genty, G. Feng, and H. Liang, "Temporal ghost imaging with random fiber lasers," Opt. Express **28**, 9957 (2020).
46. J. Lv, H. Li, Y. Zhang, R. Tao, Z. Dong, C. Gu, P. Yao, Y. Zhu, W. Chen, Q. Zhan, and L. Xu, "Few-mode random fiber laser with a switchable oscillating spatial mode," Opt. Express **28**, 38973 (2020).
47. J. Blake, H. Engan, and H. Shaw, "Analysis of intermodal coupling in a two-mode fiber with periodic microbends," Opt. Lett. **12**, 281 (1987).
48. A. Engsarkar, J. Pedrazzani, J. Judkins, P. Lemaire, N. Bergano, and C. Davidson, "Long-period fiber-grating based gain equalizers," Opt. Lett. **21**, 336 (1996).
49. M. Jiang, H. Wu, Y. An, T. Hou, Q. Chang, L. Huang, J. Li, R. Su, and P. Zhou, "Fiber laser development enabled by machine learning: review and prospect," PhotoniX **3**, 16 (2022).
50. L. Huang, J. Leng, P. Zhou, S. Guo, H. Lu, and X. Cheng, "Adaptive mode control of a few-mode fiber by real-time mode decomposition," Opt. Express **23**, 28082 (2015).
51. J. Wang, R. Chen, J. Yao, H. Ming, A. Wang, and Q. Zhan, "Random distributed feedback fiber laser generating cylindrical vector beams," Phys. Rev. Appl. **11**, 044051 (2019).